

Prospects for the Application of Nonlinear Dynamics to Spacecraft Power Systems

Yan Hong Lim and David C. Hamill

Surrey Space Centre
University of Surrey, Guildford, Surrey GU2 5XH, UK
Tel. +44 (0) 1483 259278, Fax +44 (0) 1483 259503
Email: Y.Lim@surrey.ac.uk, D.Hamill@surrey.ac.uk

ABSTRACT

Nonlinear dynamics has been successful in explaining apparently spurious behaviour in a wide variety of systems. We propose that it be applied to the analysis of spacecraft power systems. The components of space power systems are nonlinear, yet linear techniques are typically used in their dynamical analysis. This can sometimes lead to qualitatively wrong predictions of behaviour.

First, we outline some fundamental concepts of nonlinear dynamics. We then study three simple examples that model space power systems, and find phenomena that fit into the general framework of nonlinear dynamics. These include various types of bifurcation, coexisting attractors, and chaos.

Keywords: spacecraft power systems, nonlinear dynamics, stability, bifurcation, chaos.

I. INTRODUCTION

The success of a space mission depends critically on the reliability of the power system. Besides outright failures, anomalies can cause power system malfunction and may adversely affect the operation of the payloads.

Many studies have revealed the existence of nonlinear behaviour in simple electronic circuits and systems, e.g. [1]. In particular, they have often uncovered previously unsuspected bifurcation from the assumed regular mode of operation. The fact that such erratic behaviour can go unpredicted has important implications where high reliability is essential.

Power electronic circuits and systems are inherently nonlinear, because of the discontinuities caused by switching. Several groups have investigated nonlinear effects such as chaos in power converters [2, and references therein]. However, engineers continue to employ linearisation-based techniques such as small-signal modelling when investigating transient response and stability. This is tantamount to assuming that all perturbations are small: an assumption difficult to justify for strong nonlinearities such as switching discontinuities. Restricting oneself to inappropriate tools can result in incorrect predictions of system performance.

At a system level, nonlinear dynamics has succeeded in describing large-signal effects in terrestrial ac power networks [3, 4]. Loss of steady-state stability, voltage collapse and asynchronous oscillations can all be explained.

Spacecraft power systems typically comprise several interconnected dc subsystems: solar arrays, rechargeable batteries, dc-dc converters, regulators, power distribution units, and payload modules. Many of these have nonlinear characteristics. Moreover, successive generations of power systems have become larger and more complex, with increased redundancy,

digital controllers, and frequent system reconfiguration to satisfy power requirements. It is now difficult to be sure that there are no hidden anomalies, particularly when one considers parameter drifts over the design lifetime. The consequences of unwanted bifurcation could be performance degradation or unpredictable malfunctions.

The next section gives a brief exposition of the principles of nonlinear dynamics, and proceeds to identify the major nonlinearities in space power systems. We then present some detailed examples of nonlinear phenomena in simple models derived from spacecraft power systems.

II. NONLINEAR DYNAMICS AND CHAOS

The aim of *nonlinear dynamics* is to understand the complex behaviour of nonlinear systems. The following is a very brief summary of some of its main ideas.

A. Flows

A generalised continuous-time n th-order autonomous dynamical system is governed by the differential equation

$$\dot{\mathbf{x}} = \frac{d\mathbf{x}}{dt} = \mathbf{f}(\mathbf{x}) \quad \mathbf{f}: \mathfrak{R}^n \rightarrow \mathfrak{R}^n, \quad \mathbf{x}(t_0) = \mathbf{x}_0 \quad (1)$$

where $\mathbf{x}(t) \in \mathfrak{R}^n$ is the n -dimensional *state vector* at time t . In electrical systems, the state vector usually comprises the inductor currents and capacitor voltages. The derivative $\dot{\mathbf{x}}$ is known as the *vector field*. The set of all paths $\mathbf{x}(t)$ satisfying (1) is called the *flow* of the system. By choosing a particular initial condition $\mathbf{x}_0 = \mathbf{x}(0)$, we pick a single, unique *trajectory*. As t increases from zero, the state vector follows this trajectory, and the system's dynamical behaviour evolves.

B. Limit Sets

Four different types of steady-state behaviour are described here. They are termed *limit sets*, because they comprise the set of points visited by $\mathbf{x}(t)$ in the limit as $t \rightarrow \infty$.

Equilibrium points are special points in state space (denoted \mathbf{x}^*) where the vector field is zero, i.e. the state vector remains stationary. Hence $\mathbf{x}(t) = \mathbf{x}^*$ for all t . The stability of an equilibrium point is determined from the eigenvalues of the Jacobian matrix of \mathbf{f} evaluated at \mathbf{x}^* . (The Jacobian contains the partial derivatives of \mathbf{f} with respect to \mathbf{x}). Eigenvalues with a negative real part indicate contraction, and those with a positive real part, expansion. They show whether small perturbations from the equilibrium points grow or decay. If all n eigenvalues lie in the left half of the complex plane, the system is asymptotically stable. (This is similar to the stability condition for continuous linear systems; essentially, we have linearised the system about \mathbf{x}^* .)

Periodic solutions satisfy $\mathbf{x}(t) = \mathbf{x}(t + T)$ where T is some minimal period greater than zero. Their stability can be determined from their *characteristic multipliers* (Floquet multipliers) — a generalisation of the eigenvalues at an equilibrium point [5]. If the characteristic multipliers all lie within the unit circle, the periodic solution is asymptotically stable — a *limit cycle*. (This condition should be familiar from discrete linear-systems theory.)

Quasi-periodicity occurs if the spectrum of the trajectory contains two or more components whose frequencies are incommensurate, i.e. related by an irrational number.

Chaos still defies a universally accepted definition, but loosely speaking, it is a noise-like oscillation that occurs in deterministic systems and has a broadband spectrum. The trajectory is very sensitive to perturbations, and remains within a bounded region of state space. The best indicator of chaos is a positive *Lyapunov exponent* [5].

Stable limit sets are known as *attractors*. The basin of attraction is the region of state space from which the state vector is eventually captured as $t \rightarrow \infty$: in common parlance, the “catchment area” of an attractor. Chaos is associated with a fractal limit set which is infinitely complex, known as a *strange attractor*.

C. Iterated Mappings

A system can also be described by a *map*, or *mapping*. This is an algebraic function relating the state vector \mathbf{x}_m at one sampling instant to that at the next, \mathbf{x}_{m+1} . The samples can be taken in a number of ways: at regular time intervals (stroboscopic map); at particular events, e.g. maxima or minima (Lorenz map); or as $\mathbf{x}(t)$ passes through a transverse surface in state space (Poincaré map). Once obtained from the differential equations, mappings can easily be iterated to reveal the system’s dynamics [6].

An n -dimensional mapping, $\mathbf{F}: \mathfrak{R}^n \rightarrow \mathfrak{R}^n$, $\mathbf{x} \rightarrow \mathbf{F}(\mathbf{x})$ is a function that acts on the state vector \mathbf{x}_m to produce its next value \mathbf{x}_{m+1} :

$$\mathbf{x}_{m+1} = \mathbf{F}(\mathbf{x}_m), \quad m = 0, 1, 2, 3, \dots \quad (2)$$

Given an initial state \mathbf{x}_0 , the mapping can be iterated to obtain the sequence $\{\mathbf{x}_m\} = \{\mathbf{x}_0, \mathbf{x}_1, \mathbf{x}_2, \dots\}$. This is known as the *orbit* of the system.

D. Fixed and Periodic Points of Mappings

If there is an $\mathbf{x}_m = \mathbf{x}^*$ such that $\mathbf{F}(\mathbf{x}^*) = \mathbf{x}^*$ (i.e. the state vector is invariant under the mapping), then \mathbf{x}^* is known as a *fixed point* of the mapping. For a one-dimensional system, fixed points can be obtained graphically from the intersection of the line $x_{m+1} = x_m$ with the function $x_{m+1} = F(x_m)$.

The stability of a fixed point can be determined from the n eigenvalues of the Jacobian of \mathbf{F} at \mathbf{x}^* . The fixed point is stable if the spectral radius of the Jacobian is less than unity (its eigenvalues all lie within the unit circle) i.e.

$$\left\| \left(\frac{\partial \mathbf{F}}{\partial \mathbf{x}} \right)_{\mathbf{x}=\mathbf{x}^*} \right\| < 1 \quad (3)$$

For a one-dimensional system, this condition simplifies to $|F'(x^*)| < 1$.

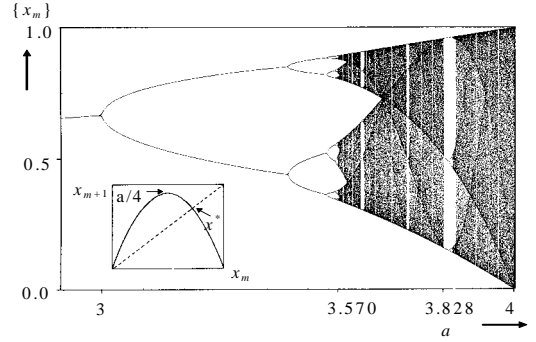


Figure 1: One-dimensional quadratic mapping (inset), and bifurcation diagram produced when a is swept from 2.9 to 4

If the state vector returns to the same point but only after two iterations of the mapping, i.e. $\mathbf{F}(\mathbf{x}^*) \neq \mathbf{x}^*$ but $\mathbf{F}(\mathbf{F}(\mathbf{x}^*)) = \mathbf{x}^*$, then \mathbf{x}^* is called a *period-2 point*. This can be generalised to period k , for which $\mathbf{F}^k(\mathbf{x}^*) = \mathbf{x}^*$ for some $k = 2, 3, 4, \dots$. The associated sequence $\{\mathbf{x}^*\} = \{\mathbf{x}_0, \mathbf{x}_1, \dots, \mathbf{x}_{k-1}\}$ is known as a *period- k orbit*, and each point in the sequence is a *period- k point*. Again, periodic orbits can be stable (attracting) or unstable, as determined by the eigenvalues of the Jacobian of \mathbf{F} evaluated at $\{\mathbf{x}^*\}$.

E. Chaos in Iterated Mappings

Chaos in iterated mappings is characterised by a sequence $\{\mathbf{x}_m\}$ which never repeats, yet remains bounded in state space. Thus the attracting chaotic orbit fills up a finite region without converging or repeating itself.

A classic one-dimensional mapping is the quadratic map

$$x_{m+1} = ax_m(1 - x_m), \quad a \in [0, 4] \quad (4)$$

A *bifurcation diagram* or *branching diagram* (Fig. 1) reveals the qualitative steady-state behaviour as a *bifurcation parameter* (in this case, a) is varied. With $a \leq 3$, $\{x_m\}$ converges to a fixed point. At $a = 3$, $\{x_m\}$ assumes a period-2 orbit. As a is increased further, periods 4, 8, 16, ... are successively born. At $a \approx 3.570$, the period becomes infinite and chaos is observed. (This is known as the period-doubling route to chaos.) Other routes include period-adding, quasi-periodicity, and intermittency [7]. For certain parameter values, stable periodic orbits appear, for example the period-3 window at $a \approx 3.828$.

F. Bifurcations

A *stationary bifurcation* occurs when a real eigenvalue changes between negative and positive (Fig. 2(a)), changing the stability of an equilibrium point. A common example is the buckling of a beam when its loading becomes excessive.

In contrast, a *Hopf bifurcation* occurs when the real part of a complex-conjugate pair of eigenvalues changes between negative and positive. A periodic solution arises. If this is stable, self-oscillation (a limit cycle) occurs (Fig. 2(b)) [8]. An

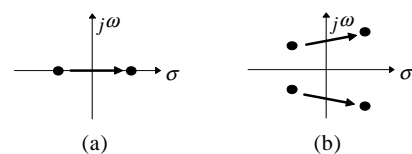


Figure 2: (a) Stationary bifurcation; (b) Hopf bifurcation

example of this is the howl-round produced by a public-address system when the gain reaches a critical level.

Bifurcations can also be characterised by the way the limit set and its stability alter with parameter changes. Some common types are saddle-node, transcritical and pitchfork bifurcations. The latter are further divided into subcritical and supercritical. Some of these will be observed below.

III. NONLINEARITIES IN SPACE POWER SYSTEMS

Next, we describe the usual nonlinearities encountered in space power systems.

A. Solar Arrays

The dc characteristic of a solar cell can be modelled mathematically by a simple relationship derived from semiconductor physics:

$$J = J_{sc} - J_o \left(\exp \frac{V}{V_T} - 1 \right) \quad (5)$$

where J is the current density, J_{sc} is the short-circuit current density (at a given level of illumination), J_o is the dark current density, V is the voltage across the cell, and V_T is the thermal voltage calculated from kT/q , k being Boltzmann's constant, q the charge on an electron, and T the absolute temperature. The relationship is clearly nonlinear.

B. Batteries

The terminal voltage of a rechargeable battery varies nonlinearly with charge. Therefore the simplest model would consist of a nonlinear capacitor [9]. Practical mathematical modelling involves many further parameters, including internal resistance and capacitance, charge and discharge rates, self-discharge and temperature.

C. Power Components

Many power electronic components are nonlinear. Power MOSFETs, bipolar transistors and diodes have intrinsically nonlinear dc characteristics, and also nonlinear capacitances. Transformers, chokes, and magnetic amplifiers have nonlinear inductances. Control elements such as pulse-width modulators, current-mode controllers and phase-locked loops are also inherently nonlinear.

D. Dc-Dc Converters

There is now over ten years of literature describing bifurcations and chaos in dc-dc converters of various topologies operating with different control schemes. It is probable that all topologies are capable of chaos, given the right conditions.

For example, a simple voltage-controlled buck converter was

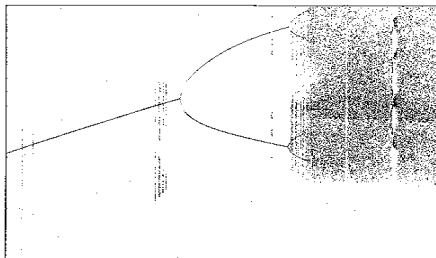


Figure 3: Simulated bifurcation diagram for the buck converter in CCM: $\{v_m\}$ plotted against $V_1 \in \{15V, 40V\}$

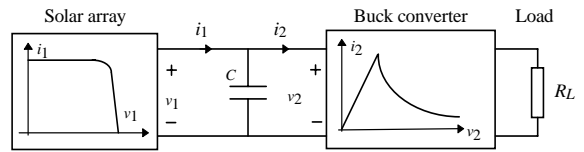


Figure 4: Schematic of a first-order power system

studied by conventional state-space averaging, and appeared stable over a wide input range [2]. When the tools of nonlinear dynamics were applied, the same circuit revealed a surprising range of behaviour: subharmonics, intermittency, chaos, coexisting attractors, and even narrow bands of chaotic behaviour embedded in an otherwise stable region. A simulated bifurcation diagram is shown in Fig. 3, and was confirmed by experimental observations. Considering that the buck converter and its derivatives are extremely common, and are widely thought to be well understood, this does not inspire confidence in linear models!

IV. BUS VOLTAGE COLLAPSE

To demonstrate the value of nonlinear dynamics, we shall describe some familiar effects in space power systems by investigating simplified but relevant models.

Let us first consider a simple first-order system comprising a solar array, a reservoir capacitor and a buck dc-dc converter, as shown in Fig. 4. For illustrative purposes we assume that there is no battery, so the spacecraft is powered in sunlight only. A similar spacecraft power system of second order was previously studied by other workers [10].

Rather than use the solar-cell characteristic of (5), we simplify calculations by modelling the solar array by the polynomial

$$i_1 = \alpha I_{sc} \left(1 - \left(\frac{v_1}{V_{oc}} \right)^p \right), \quad 0 \leq v_1 \leq V_{oc}, \quad 0 \leq i_1 \leq I_{sc} \quad (6)$$

where i_1 and v_1 are the array's terminal current and voltage, I_{sc} is the short-circuit current, V_{oc} is the open circuit voltage, and the exponent $p = 33$ is chosen to approximate closely the dc characteristic of a real solar array.

The coefficient α denotes the relative solar illumination ($0 \leq \alpha \leq 1$). In the following analysis, we use α as a bifurcation parameter.

The solar array feeds a reservoir capacitor and a regulated buck converter, assumed to operate in CCM, which has a resistive load R_L . The converter has two modes of operation, depending on its input voltage. In the desirable mode, the input voltage is sufficient to produce a regulated output voltage, resulting in a constant-power input characteristic. However, when the input voltage is too low, the buck converter's switch closes continuously, and its input characteristic becomes simply that of R_L . This mode is undesirable because the output voltage is unregulated.

The converter's input characteristic is

$$i_2 = \begin{cases} \frac{V_{ref}}{R_L v_2} & \text{if } v_2 \geq V_{ref} \quad (\text{desirable mode}) \\ \frac{v_2}{R_L} & \text{if } v_2 < V_{ref} \quad (\text{undesirable mode}) \end{cases} \quad (7)$$

where i_2 and v_2 are the input current and voltage and V_{ref} is the desired output voltage. Since $v_2 = v_1$, the system equation is

$$\frac{dv_1}{dt} = \frac{i_1(v_1) - i_2(v_1)}{C} = f(v_1) \quad (8)$$

where $i_1(v_1)$ is given by (6) and $i_2(v_1)$ by (7). We obtain the equilibrium points $\{v_1^*\}$ by setting $f(v_1) = 0$ and solving for v_1 . We use the following parameters: $I_{sc} = 4\text{A}$, $V_{oc} = 46.2\text{V}$, $V_{ref} = 14\text{V}$, $R_L = 3.92\Omega$, $C = 250\mu\text{F}$. Two cases are considered: $\alpha = 1$ and $\alpha = 0.5$ (full and half illumination). There may be one, two or three equilibrium points, depending on the parameter values (see Fig. 5). Table I shows numerical results.

Table I: Equilibrium points

α	Undesirable mode		Desirable mode	
	v_1^*	$i_1^* = i_2^*$	v_1^*	$i_1^* = i_2^*$
0.50	7.840	2.000	25.000	2.000
			45.082	1.109
1.00	–	–	45.755	1.092

The stability of the equilibrium is determined by evaluating df/dv_1 at v_1^* (for a first-order system, the equivalent of the eigenvalue of the Jacobian). Table II summarises the results. Negative values indicate stability; positive ones, instability.

Table II: Stability and mode of equilibrium points

α	Label	v_1^*	df/dv_1	Stability	Mode
0.50	A	7.840	-1020.41	stable	undesirable
	B	25.000	+319.99	unstable	desirable
	C	45.082	-2510.87	stable	desirable
1.00	D	45.755	-8289.07	stable	desirable

At $\alpha = 1$ (full illumination), there is a single stable equilibrium point, D in Fig. 5, where the buck converter operates in its desirable mode. As α is decreased, this point moves to C, but two additional equilibria emerge, A and B. Point B is unstable, but point A is stable and occurs in the undesirable mode of operation.

To investigate in more detail, the system equation (8) was investigated numerically using the XPPAUT program [11]. In this package, data from the XPP differential-equation solver is fed to AUTO [12], producing a bifurcation diagram, Fig. 6.

Two interesting illumination levels are $\alpha = 0.3102$ and $\alpha =$

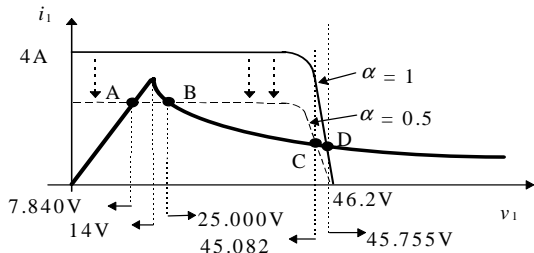


Figure 6: V - I characteristics, showing equilibrium points A, B, C and D

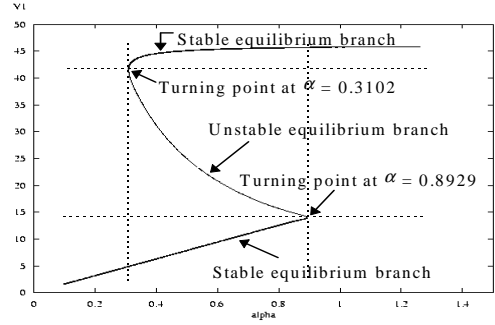


Figure 5: Bifurcation diagram of v_1^* against α , showing hysteresis for $0.3102 < \alpha < 0.8929$

0.8929. Here a saddle-node stationary bifurcation occurs, at a *turning point* where two branches of equilibria meet — stable and unstable. Globally, these values of α delimit a range in which two values of array voltage are stable and one is unstable. Within the range, either of the two stable equilibria might be chosen, depending on the initial conditions. This phenomenon is well known as *hysteresis*. A large disturbance might flip the system to its other stable equilibrium, where it would remain. This is a simple example of *coexisting attractors*. The unstable branch separates the basins of attraction of each stable branch.

If R_L is taken as the bifurcation parameter instead of α (which is set to one), the range $1.215\Omega < R_L < 3.5\Omega$ is now associated with hysteresis.

In normal operation, the system sits on the upper stable branch. Either α or R_L (or both) may vary. If the input power is insufficient to provide the load power demanded, the system jumps to the lower stable branch, where it remains. This effect, *bus voltage collapse*, is a well known hazard of spacecraft power system operation. To escape from it, R_L has to be increased (beyond 3.5Ω at full illumination) by turning off payloads: *load shedding*.

V. SPURIOUS OSCILLATIONS

We extend the model to higher dimensions by including two further filter components as shown in Fig. 7. The system equations are now:

$$\frac{dv_1}{dt} = \frac{i_1(v_1) - i_L}{C_1} = f_1(v_1, i_L, v_2) \quad (9)$$

$$\frac{di_L}{dt} = \frac{v_1 - i_L R_s - v_2}{L} = f_2(v_1, i_L, v_2) \quad (10)$$

$$\frac{dv_2}{dt} = \frac{i_L - i_2}{C_2} = f_3(v_1, i_L, v_2) \quad (11)$$

which is of the form $\dot{\mathbf{x}} = \mathbf{f}(\mathbf{x})$. With parameter values $C_1 = 50\mu\text{F}$, $C_2 = 350\mu\text{F}$, $L = 700\mu\text{H}$ and $R_s = 0.2\Omega$, the equilibrium points $\{\mathbf{x}^*\}$ are found by setting f_1 , f_2 and f_3 simultaneously to

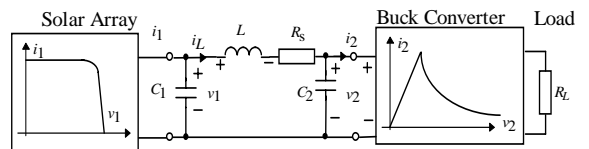


Figure 7: Power system including third-order filter

zero. See Fig. 8 and refer to Table III for results.

Table III: Equilibrium points

Undesirable mode ($v_2 < V_{ref}$)						
α	Label	i_1^*	v_1^*	i_L^*	v_2^*	i_2^*
0.25	D ₁	1.00	4.12	1.00	3.92	1.00
0.50	C ₁	2.00	8.24	2.00	7.84	2.00
0.75	B ₁	3.00	12.36	3.00	11.76	3.00
1.00	—	—	—	—	—	—
Desirable mode ($v_2 \geq V_{ref}$)						
α	Label	i_1^*	v_1^*	i_L^*	v_2^*	i_2^*
0.25	—	—	—	—	—	—
0.50	C ₂	2.00	25.40	2.00	25.00	2.00
	C ₃	1.114	45.10	1.114	44.88	1.114
0.75	B ₂	3.00	17.72	3.00	16.67	3.00
	B ₃	1.102	45.67	1.102	45.45	1.102
1.00	A ₃	1.098	45.75	1.098	45.53	1.098

To investigate the stability, we examine the eigenvalues $\{\lambda_1, \lambda_2, \lambda_3\}$ of the Jacobian at each equilibrium point (Table IV). Besides the stationary bifurcation we saw in the first-order system, Table IV shows evidence of a Hopf bifurcation.

Table IV: Eigenvalues of the Jacobian at the equilibrium points

α	Label	Eigenvalues			Stability
		λ_1	λ_2	λ_3	
0.25	D ₁	-2345.2 -j4812.0	-2345.2 +j4812.0	-678.2	stable
0.50	C ₁	-2345.2 -j4812.0	-2345.2 +j4812.0	-678.3	stable
	C ₂	+564.5 -j5431.4	+564.5 +j5431.4	+204.4	unstable
	C ₃	-21.4 -j5462.6	-21.4 +j5462.6	-1615.2	stable
0.75	B ₁	-2345.1 -j4812.0	-2345.1 +j4812.0	-678.3	stable
	B ₂	+1422.3 -j5109.5	+1422.3 +j5109.5	+487.3	unstable
	B ₃	-86.84 -j5362.1	-86.84 +j5362.1	-3841.2	stable
1.00	A ₃	-88.28 -j5297.9	-88.28 +j5297.9	-5575.8	stable

As before, we generate a bifurcation diagram with α as the bifurcation parameter, Fig. 9. Once again, we witness hysteresis. The range is now $0.3113 < \alpha < 0.8998$. The values are slightly higher, because $R_s > 0$. There are two further interesting values of illumination: $\alpha = 0.4534$ and $\alpha = 0.8997$. Starting at these Hopf points, AUTO now traces the branches of the periodic solutions, which can again be either stable (limit cycles) or unstable.

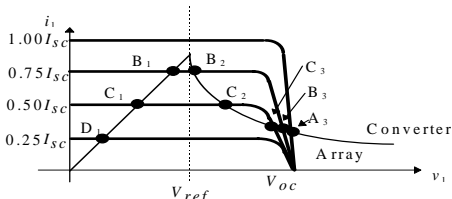


Figure 8: Converter and solar array V - I characteristics with varying illumination factor α

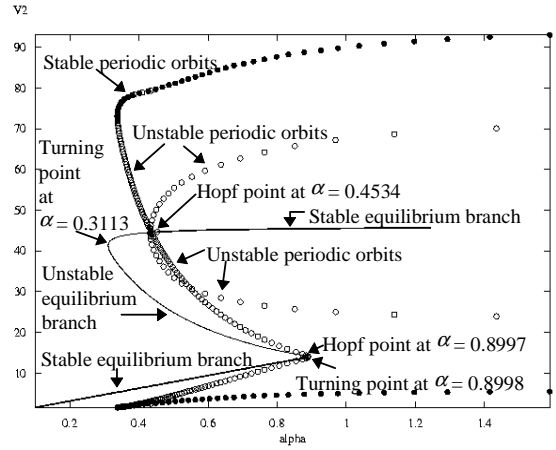


Figure 9: Bifurcation diagram of v_2^* against α showing hysteresis between $0.3113 < \alpha < 0.8998$, two Hopf points at $\alpha = 0.3434$ and $\alpha = 0.8997$, where subcritical Hopf bifurcations occur. Filled dots represent stable periodic orbits; open dots represent unstable periodic orbits

These are *subcritical Hopf bifurcations*, as periodic-solution branches emanate from the stable-equilibrium branches. Unstable at first, they turn and become stable (limit cycles). In the range $0.4534 < \alpha < 0.8997$, three attractors coexist: two stable equilibria and a stable limit cycle; also there are also two unstable periodic solutions and an unstable equilibrium, making for very complex transient dynamics.

The range $\alpha > 0.35$ is of particular engineering concern, because besides the desired stable equilibria, stable limit cycles exist, perhaps unsuspected. Suppose the system is operating as intended, on the upper stable equilibrium branch at $\alpha = 0.95$, say. With a large perturbation, the system might cross into the basin of attraction of the limit cycle, bursting into sustained large-amplitude oscillation. Coexisting attractors of this type are a serious threat to reliable operation, and may cause malfunctions or failure.

VI. CHAOS

In our third model (Fig. 10), an undervoltage lockout is incorporated in the converter. Such circuits are commonly employed to prevent overdischarge of batteries during eclipse, or to ensure that converters operate in their proper mode so that the payloads do not receive an unregulated voltage. When its input voltage is too low, the converter is disconnected; when the voltage recovers, it is automatically reconnected. Some hysteresis is needed between the disconnect and reconnect voltages to prevent chattering.

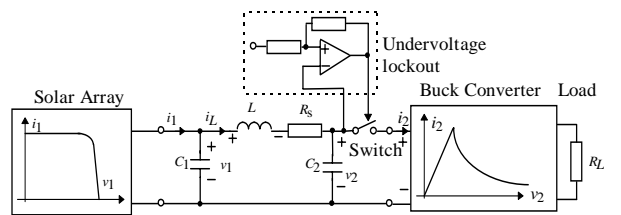


Figure 10: Schematic of power system with third-order filter incorporating undervoltage lockout

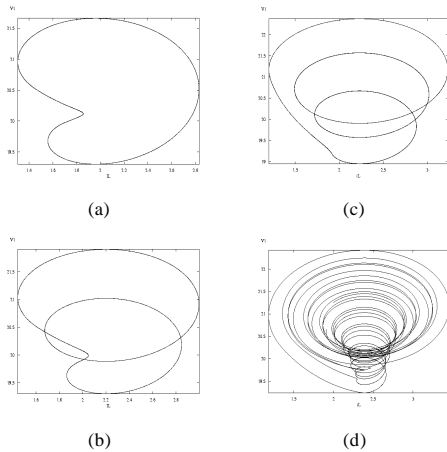


Figure 12: State trajectories of v_1 against i_L at (a) $\alpha = 0.49$, (b) $\alpha = 0.55$, (c) $\alpha = 0.558$, (d) $\alpha = 0.597$

In this model, $L = 250\mu\text{H}$, $C_1 = 120\mu\text{F}$, $C_2 = 250\mu\text{F}$, and the hysteresis thresholds are set to $v_2 = 19\text{V}$ (disconnect) and 21V (reconnect). For increasing illumination levels, Fig. 11 shows steady-state simulation results of v_1 against i_L , and Fig. 12 shows the corresponding $v_1(t)$ waveform. In (a) there is a limit cycle for $\alpha = 0.490$. In (b), with $\alpha = 0.550$, the period has doubled, and in (c), with $\alpha = 0.558$, it has trebled. Further period-doubling occurs until in (d), with $\alpha = 0.597$, the behaviour is chaotic. Thus the system follows the classic period-doubling route to chaos.

The chaotic operation can be described qualitatively as follows. First, let us temporarily ignore the undervoltage lockout. The constant-power input characteristic of the converter presents a negative resistance, which excites the resonance between the inductance and effective capacitance, causing self-oscillation near the resonant frequency. If instead we ignore L for the moment, the hysteresis permits a relaxation oscillation, as the capacitors discharge during voltage collapse, then recharge from the solar array while the converter is locked out. This oscillation has its own frequency, determined by the capacitances and the charge/discharge currents. In general, these two oscillations are at incommensurate frequencies, so quasi-periodicity might occur. But there is a nonlinear interaction between the two oscillations. They can lock together, resulting in period multiplication; or they can synchronise intermittently, causing chaos [13].

The system exhibits sensitive dependence on initial conditions, a fundamental property of chaotic behaviour. When the simulations are repeated with initial conditions differing by just 0.01V , the trajectories rapidly diverge from each other.

The Poincaré map of Fig. 13 was constructed by plotting v_1 against i_L , sampled each time v_2 crosses the 20V level. The fractal nature of the attractor is further evidence of chaos.

VII. CONCLUSION

Various aspects of spacecraft power system stability have been studied with the aid of simplified models. The simulation results revealed hysteresis, Hopf bifurcation leading to limit cycles, period multiplication and chaotic behaviour. This approach can potentially shed new light on some familiar but poorly understood effects, including bus voltage collapse, spurious oscillations, and chaotic “noise”. These phenomena,

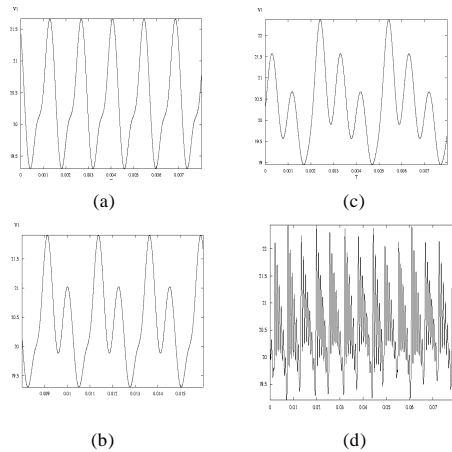


Figure 13: $v_1(t)$ waveform at (a) $\alpha = 0.49$, (b) $\alpha = 0.55$, (c) $\alpha = 0.558$, (d) $\alpha = 0.597$

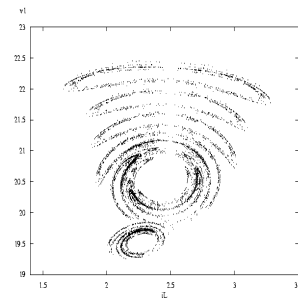


Figure 11: Poincaré mapping sectioned at $v_2 = 20\text{V}$

which might result in power system malfunction or mission failure, can be fully understood and (we hope) avoided, by applying the concepts and tools of nonlinear dynamics.

REFERENCES

- [1] T. Matsumoto, “Chaos in electronic circuits”, *Proc. IEEE*, vol. 75, no. 8, pp. 1033-1056, Aug. 1987.
- [2] D.C. Hamill, “Power electronics : a field rich in nonlinear dynamics”, *Workshop on Nonlinear Dynamics of Electronic Systems*, Dublin, pp. 164-179, July 1995.
- [3] M. Wildberger, “Stability and nonlinear dynamics in power systems”, *EPRI Journal*, pp. 36-39, June 1994.
- [4] H.G. Kwantny, A.K. Pasrija and L.Y. Bahar, “Static bifurcations in electric power networks: loss of steady-state stability and voltage collapse”, *IEEE Trans. on Circuits and Systems*, vol. 33, no. 10, pp. 981-999, Oct. 1986.
- [5] T.S. Parker and L.O. Chua, “Chaos: a tutorial for engineers”, *Proc. IEEE*, vol. 75, no. 8, pp. 982-1008, Aug. 1987.
- [6] D.C. Hamill, J.H.B. Deane and D.J. Jefferies, “Modeling of chaotic dc-dc converters by iterated nonlinear mappings”, *IEEE Trans. on Power Electronics*, vol. 7, no. 1, pp. 25-36, Jan. 1992.
- [7] F.C. Moon, *Chaotic and Fractal Dynamics*, Wiley, 1992.
- [8] R. Seydel, *From Equilibrium to Chaos: Practical Bifurcation and Stability*, Elsevier, 1988.
- [9] H.J.N. Spruijt, “Possible battery cell model topologies”, *Euro. Space Power Conf.*, Graz, pp. 671-676, Aug. 1993.
- [10] B.H. Cho, J. R. Lee and F. C. Lee, “Large signal stability analysis of spacecraft power processing systems”, *IEEE Trans. on Power Electronics*, vol. 3, no. 1, pp. 44-54, Jan. 1988.
- [11] B. Ermentrout, *XPPAUT*, Univ. of Pittsburg (<http://www.pitt.edu/~phase/>)
- [12] E. Doedel, *AUTO*, Concordia Univ. (<ftp://ftp.cs.concordia.ca/pub/doedel/auto/>)
- [13] Y.S. Tang, A.I. Mees and L.O. Chua, “Synchronization and chaos”, *IEEE Trans. on Circuits and Systems*, vol. 30, no. 9, pp. 620-626, Sep. 1983.